



Thermo-kinetic modelling of the acidic leaching of anorthosite: Key learnings toward the conception of a sustainable industrial process

Thomas Neron, Laurent Cassayre, Xuan Zhuo, Marie-Hélène Manero, Florent Bourgeois, Anne-Marie Billet, Carine Julcour-Lebigue

► To cite this version:

Thomas Neron, Laurent Cassayre, Xuan Zhuo, Marie-Hélène Manero, Florent Bourgeois, et al.. Thermo-kinetic modelling of the acidic leaching of anorthosite: Key learnings toward the conception of a sustainable industrial process. Minerals Engineering, 2022, 180, pp.107500. 10.1016/j.mineng.2022.107500 . hal-03713327

HAL Id: hal-03713327

<https://hal.science/hal-03713327>

Submitted on 4 Jul 2022

HAL is a multi-disciplinary open access archive for the deposit and dissemination of scientific research documents, whether they are published or not. The documents may come from teaching and research institutions in France or abroad, or from public or private research centers.

L'archive ouverte pluridisciplinaire **HAL**, est destinée au dépôt et à la diffusion de documents scientifiques de niveau recherche, publiés ou non, émanant des établissements d'enseignement et de recherche français ou étrangers, des laboratoires publics ou privés.









Open Archive Toulouse Archive Ouverte (OATAO)

OATAO is an open access repository that collects the work of Toulouse researchers and makes it freely available over the web where possible

This is an author's version published in: <http://oatao.univ-toulouse.fr/29103>

Official URL: <https://doi.org/10.1016/j.mineng.2022.107500>

To cite this version:

Neron, Thomas  and Cassayre, Laurent  and Zhuo, Xuan and Manero, Marie-Hélène  and Bourgeois, Florent  and Billet, Anne-Marie  and Julcour-Lebigue, Carine  *Thermo-kinetic modelling of the acidic leaching of anorthosite: Key learnings toward the conception of a sustainable industrial process.* (2022) Minerals Engineering, 180. 107500. ISSN 0892-6875

Any correspondence concerning this service should be sent
to the repository administrator: tech-oatao@listes-diff.inp-toulouse.fr

Thermo-kinetic modelling of the acidic leaching of anorthosite: Key learnings toward the conception of a sustainable industrial process

Thomas Neron, Laurent Cassayre, Xuan Zhuo, Marie-Hélène Manero, Florent Bourgeois, Anne-Marie Billet, Carine Julcour*

Laboratoire de Génie Chimique, Université de Toulouse, CNRS, INP, UPS, Toulouse, France

ARTICLE INFO

Keywords:

Hydrometallurgy
Acid leaching
Geochemical modelling
Dissolution kinetics
Shrinking core model
Batch-to-continuous processing

ABSTRACT

The world is facing critical technological and environmental challenges in the production of basic materials in high demand, such as aluminium and silica, whose processes were developed long ago. New production routes, involving using alternative resources and innovative technological solutions, are needed to secure access to these base materials at a lower cost to the environment, in terms of waste and carbon footprint. The European project ALSiCal is currently investigating an environmentally friendly multi-step process for producing alumina and silica from anorthosite, an abundant feldspar mineral. The present paper focuses on the modelling strategy of the dissolution of anorthosite in concentrated hydrochloric acid, which is the first step of the ALSiCal process. The objectives of this study are (i) to give a reliable first-level prediction of the product speciation in the aqueous and solid phases, (ii) to provide the sensitivity of the process to key operating variables, and finally, (iii) to evaluate the performance of both batch and continuous leaching processes. The proposed methodology is based on the coupling of geochemical equilibrium simulations and particle reaction models, using different computational tools and relevant literature data. This makes it possible to select the favourable operation window and process configuration for the quantitative extraction of aluminium in solution and the production of amorphous silica with an acceptable purity for large-market applications.

1. Introduction

1.1. Context

Due to its multiple applications (e.g. in transportation, construction, containers and packaging, electrical products, household goods), aluminium is one of the most used non-renewable resources. It is also currently the second most produced metal, after iron. Aluminium production has increased by more than 30-fold since the end of the Second World War (Vidal et al., 2017). It now exceeds 64 million tons per year (USGS, 2020) and it is expected to increase significantly in the future. Indeed, the demand for metal (including aluminium) used in electric batteries is expected to increase by 1000% over the next thirty years (European Economic and Social Committee, 2020).

Alumina (Al_2O_3) is the raw material used to produce aluminium with a high temperature electrolysis process. It is mainly obtained by leaching an alumina-containing ore known as bauxite. The most common process used to obtain alumina from bauxite is the one developed in 1887 by

Bayer (Bayer, 1888, 1894). It is based on leaching by caustic soda at high temperatures (from 150 °C to 250 °C depending on the mineralogy of aluminium bearing phases in the bauxite (Kaußen and Friedrich, 2018; Mihajlović et al., 2014)) and high pressure (~35 bar at 240 °C). After a filtration step to remove impurities, the liquor is precipitated to obtain aluminium hydroxide $\text{Al}(\text{OH})_3$, which is then calcined to obtain alumina. Alumina preparation from bauxite ore is thus the result of a complex process that generates large quantities of hazardous by-products, commonly called “red mud”. The production of one ton of aluminium yields one to four tons of red mud. It is usually landfilled even though it contains heavy metals such as arsenic (As), lead (Pb), titanium (Ti) or chromium (Cr). Red mud has become a hardly acceptable waste in an increasingly tense environmental context (Mayes et al., 2016). In addition, the quality of bauxite production is decreasing, contributing to an increase in prices for the whole aluminium value chain. Finally, the main bauxite production sites are located in only four countries: Australia (29%), Guinea (19%), China (19%) and Brazil (13%) (World Bank, 2020). It may create strategic tensions for American

* Corresponding author.

E-mail address: carine.julcour@ensiacet.fr (C. Julcour).

or European supply chains.

In this context, alternative alumina production processes using other sources of Al-bearing minerals than bauxite must be considered. Among these minerals, anorthosite is one of the most promising alternatives. It is a plagioclase feldspar found in many places of the world, including Greenland, Norway and Canada (Herz, 1969). Anorthosite has been considered a suitable raw material for aluminium production for decades. For instance, from 1976 to 1982, major geological investigations and process development were carried out in the context of the Norwegian Anortal process (Gaudernack et al., 1978; Braaten, 1991; Wanvik, 2000). The operation consists in leaching anorthosite with strong acids, the most suitable one being hydrochloric acid (HCl) (Wanvik, 2010). The leachate is then processed through successive crystallization (by gaseous HCl sparging or evaporation) and purification (NaCl removal) steps to selectively precipitate aluminium chloride hydrate ($\text{AlCl}_3 \cdot 6\text{H}_2\text{O}$). Finally, the latter is calcined to produce alumina. However, due to the high costs of acid and energy required for the calcination step (about 25% more than for the aluminium hydroxide calcination step in the Bayer process), this process was not economically viable for replacing bauxite. The main outlets for anorthosite have thus been for aluminium chemicals, excluding metal (Velduyzen, 1995).

In recent years, the large increase in demand for aluminium, the decrease of bauxite quality, as well as the desire to relocate production to European and North American countries, have spurred new interest in the use of anorthosite. In particular, the Aranda-Mastin process (Aranda and Mastin, 2015) proposes to dissolve crushed anorthosite in a concentrated HCl solution at low pressure (<10 bar) and moderate temperature (<180 °C). This leaching step makes it possible to extract aluminium, calcium and sodium in solution, while silica is only yielded as a solid by-product. Moreover, the Aranda-Mastin process includes the subsequent recovery of HCl by distillation and amine extraction. It also uses CO_2 to produce precipitated calcium carbonates.

In line with this technology, the European project AlSiCal is currently investigating a multi-step process which uses anorthosite as the starting material to produce valuable materials (including alumina and amorphous silica). This process could avoid solid waste and reduce CO_2 emissions during production.

The first stage of the process, the leaching of the ore, is not well defined because only few experimental studies have been carried out. The available reports on anorthosite dissolution (Gjelsvik, 1980; Velduyzen, 1995) emphasize the sensitivity of the aluminium extraction yield to the ore properties. In particular, Gjelsvik (Gjelsvik, 1980) studied the leaching of aluminium with hydrochloric acid (6 N) at 105 °C. The study concluded that plagioclase solubility mainly depends on the albite-anorthite balance in the solid solution. A minimum anorthite content of 50 wt% was reported for the solubilisation of the ore. In this context, Gudvangen anorthosite (with an anorthite/albite stoichiometric ratio of ca. 65/35), investigated in the Norwegian Anortal process, was found to be a particularly well-suited material and it became a benchmark in subsequent studies (Velduyzen, 1995). It is also worth noting that the latest developments in the Anortal process include counter-current leaching of millimetre-sized particles by 19% HCl at 6 bar and 150 °C in vertical columns (Braaten, 1991).

However, aside from these technical reports, not much is known about anorthosite leaching. Consequently, this study gathers the available experimental data and provides a chemically-oriented model to account for the phenomena occurring in a leaching reactor. Its objective is to investigate the sensitivity of leaching performance to key operating variables in order to design a continuous process.

1.2. Scope and objectives of the model

The main objective of the model is to calculate the extraction yield of aluminium as well as the other main elements composing anorthosite (Ca, Si, Na), as a function of time, for a given initial system defined by its composition (amount of solid, water and HCl), temperature and particle

size distribution of the solid. The second major output concerns the nature and composition of the solid phases, since the process also targets the production of amorphous precipitated silica with acceptable purity for large-scale industrial applications.

Based on the aforementioned published experimental studies (later analysed in section 3.1), an operating temperature of up to 160 °C was considered, while the HCl concentration range was restricted to the azeotropic concentration (20 wt%) to minimize acid loss and facilitate its recycling in the subsequent process steps (see paragraph 2.1). Particle size was limited to the sub-millimetric range since most of the available kinetic data involve finely ground fractions. The composition of the anorthosite ore considered in this work is a mixture of anorthite and albite ($\text{CaAl}_2\text{Si}_2\text{O}_8$)_x($\text{NaAlSi}_3\text{O}_8$)_{1-x} with $x = 0.65$, referred to as $\text{Ca}_{0.65}\text{Na}_{0.35}$ in the rest of the paper. The presence of impurities, such as iron oxides, was not considered since this issue can be at least partly mitigated by preliminary magnetic separation (Wanvik, 2010).

In the aim of building a dissolution model and recommending operating procedures for the leaching of anorthosite, it is essential to distinguish the effect of operating conditions on the outcome of the leached elements. Thus, these involve system thermodynamics on one hand, and process kinetics on the other hand. The two are closely interrelated: dissolution kinetics controls the amount of elements going into the aqueous solution, while thermodynamics influence the surface reaction rate (through proton activity) and the transformation of the dissolved species (in solution and/or as new precipitated phases).

Our modelling approach successively addressed the thermodynamic description of the system and the kinetics of the dissolution process. We implemented classical chemical engineering models (shrinking particle / shrinking core models) in a suitable thermodynamic simulation environment. This approach was previously developed for a mineral carbonation process (Julcour et al., 2020). In each stage, the influence of relevant parameters (temperature, acid concentration, ore concentration and/or particle size distribution) was examined. Moreover, to overcome the lack of information on the possible by-products formed during the leaching process, two different tools were applied for equilibrium calculations (cf. paragraph 2.2):

- the OLI Studio-Stream Analyzer (version 10.0.2), a commercial software from OLI system Inc (Anderko et al., 2002),
- the PHREEQC software, an open source geochemical code developed by USGS (Parkhurst and Appelo, 2013).

In addition to using specific models to represent the electrolyte solution, these software packages are provided with distinct geochemical databases. Thus, the comparison of their predictions will give more robustness to the delineated operating window.

Finally, different reactor configurations were evaluated to operate the dissolution, as a single stirred tank or a multistage continuous (co-current or counter-current) process.

2. Thermodynamic model

2.1. Composition of the system

Hydrochloric acid leaching of anorthosite involves the use of the H_2O -HCl-Al-Ca-Si-Na multi-element system, whose full thermodynamic description is a great challenge.

The bubble temperature of the HCl- H_2O mixture is represented in Fig. 1, as a function of the amount of HCl added to 1 kg of water up to 600 g of HCl (37.5 wt% of HCl), at a total pressure of 1, 3 and 5 bar. The equilibrium curves were calculated using the OLI software and the AQ database (see next section for further details), and validated with the data compiled in the recent article of Saravi et al. (Saravi et al., 2018). As illustrated in Fig. 1, there is a strong limitation of the HCl content that can be used in the leaching solution. For instance, at atmospheric pressure, the composition with the highest bubble temperature

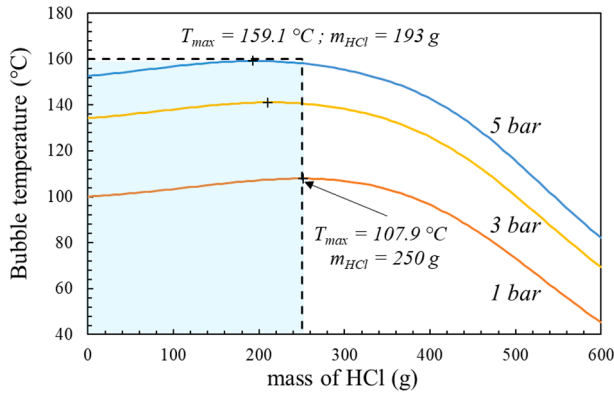


Fig. 1. Bubble temperature of the HCl-H₂O mixture at 1, 3 and 5 bar (1 kg of water; computed with OLI/AQ); the coloured area indicates the temperature and HCl content limits taken into account in the model.

(107.9 °C) which will minimize HCl volatilization, is 20 wt% of HCl. At higher HCl content, the boiling temperature drops sharply. At higher pressure, the azeotrope coordinates shift towards higher temperature and lower HCl contents.

In the rest of this section, we present the thermodynamic model, database and computational tool which were selected for the leaching model, based on the following requirements:

- (i) an accurate representation of the solubility of major solid phases to explore the influence of operating conditions (25 °C < T < 160 °C, HCl up to 20 wt%) on the leaching process;
- (ii) an accurate representation of proton (H⁺) activity in the aqueous phase for kinetic modelling of the leaching process,
- (iii) the possibility to combine the equilibrium calculations in a computational tool to implement kinetic modelling.

2.2. Aqueous phase description by activity coefficient model

2.2.1. Thermodynamic frameworks and computational tools

The main issue related to solid-liquid equilibria calculations in the H₂O-HCl-Al-Ca-Si-Na system is the description of the aqueous phase with high concentration of ionic species, as well as the large number of solid phases that may be stable. Although the choice of thermodynamic models for the description of concentrated electrolyte solutions is still the subject of controversy (May and Rowland, 2017), we only considered activity coefficient models, which are the most adapted for solid-liquid equilibria calculations.

Table 1

Activity coefficient models and associated databases considered to describe the aqueous phase for acid leaching of anorthosite.

Model name	Main equation	Ionic strength range	Associated database
B-dot	$\log \gamma_i = \frac{A_{DH(T)} Z_i^2 \sqrt{I}}{1 + B_{DH(T)} a_i \sqrt{I}} + b_{(T)} I$	$I \leq 1M$	Thermoddem (Blanc et al., 2012)
Specific ion Interaction Theory (SIT)	$\log \gamma_i = \frac{A_{DH(T)} Z_i^2 \sqrt{I}}{1 + B_{DH(T)} a_i \sqrt{I}} + \sum_k \epsilon_{(T)}(i; k) m_k$	$I \leq 5M$	Thermochimie (Giffaut et al., 2014)
Bromley-Zemaitis	$\log \gamma_{\pm} = \frac{A Z_+ Z_- \sqrt{I}}{1 + \sqrt{I}} + \frac{(0.06 + 0.6B) Z_+ Z_- \sqrt{I}}{\left(1 + \frac{1.5}{ Z_+ Z_- } I\right)^2} + BI + CI^2 + D I^3$	$I \leq 30M$	OLI Aqueous (Anderko et al., 2002; Bromley, 1973; Zemaitis, 1980)
Pitzer	$\ln \gamma_i = \frac{1}{RT} \left(\frac{\partial G^E}{\partial n_i} \right) \frac{G^E}{RT w_i} f(I) + \sum_i \sum_j \lambda_{(I)}(i; j) m_i m_j + \sum_i \sum_j \sum_k \mu(i; j; k) m_i m_j m_k$	$I \leq 10 - 12M$	Christov & Moller (Christov and Moller, 2004)

With γ_i (γ_{\pm}) the (mean) activity coefficient; T the absolute temperature; R the gas constant; $A_{DH(T)}$ and $B_{DH(T)}$ temperature-dependent parameters of the Debye-Hückel model; Z_i the charge of the aqueous species i ; a_i and $b_{(T)}$ parameters of the B-dot model; I the ionic strength; m_i the molality of the aqueous species i ; $\epsilon_{(T)}(i; k)$ interaction parameters of the SIT model; A, B, C, D parameters of the Bromley-Zemaitis model; $\lambda_{(I)}(i; j)$, $\mu(i; j; k)$ interaction parameters of the Pitzer model.

Our model selection relies on four different activity coefficient models, whose main equations are presented in Table 1, along with the main thermodynamic databases which contain model parameters. As we mentioned above, two computational tools were used to implement the thermodynamic calculations: the OLI Studio (v10.0) from OLI Systems (Anderko et al., 2002) with its Aqueous Geochemical (AQ-GE) thermodynamic database, and the PHREEQC software (v3.3) from USGS (Parkhurst and Appelo, 2013), which runs all the other models mentioned in Table 1. One of our requirements was to build a kinetic dissolution model with flexibility on the dissolution mechanism (see section 3). As such, we chose the PHREEQC software to implement our model, and used OLI Studio as a benchmark for equilibrium calculations. As developed in the following sections, the relevance of the models from Table 1 was first evaluated on the HCl-H₂O system. The model selection was then based on the availability of model parameters to represent the multi-element aqueous system, and finally discussed towards solid-liquid equilibria, including comparison with published solubility data related to amorphous silica.

2.2.2. Thermodynamic description of the HCl-H₂O system

As described in a recent assessment of the thermodynamic properties of the HCl-H₂O system on the whole composition range (Saravi et al., 2018), the addition of HCl to water, up to about 50 wt%, forms a one-liquid system with H₂O, H₃O⁺ and Cl⁻ as dominant species. At higher HCl concentrations, the content of molecular HCl_(aq) increases, which eventually forms a non-miscible phase when concentration reaches 60 to 70 wt% depending on temperature. Since the maximal HCl concentration considered in this work is about 20 wt%, we did not consider the 2-liquid phase region nor the HCl_(aq) species in our thermodynamic description.

A comparison of the activity coefficient of H⁺ ($\gamma_{(H^+)}$) as a function of the molality of HCl, calculated by the above-mentioned models at 25 and 100 °C, is provided in Fig. 2. Available experimental data (Mesmer and Holmes, 1992; Robinson and Harned, 1941) are also reported. This evaluation shows that, apart from the B-dot model which does not represent satisfactorily $\gamma_{(H^+)}$ for HCl molalities above approximatively 2 mol/kg, the three other models provide rather close values up to 7 mol/kg and 100 °C and are consistent with available data. Specifically, the SIT model, using the temperature dependent (H⁺ Cl⁻) pair interaction proposed by Xiong (Xiong, 2006), is as accurate as the Pitzer and Bromley-Zemaitis models. Given the small amount of parameters required by the SIT model, and the ease of implementation and combination with larger existing databases within the PHREEQC software, we selected the SIT model to describe the HCl-H₂O system.

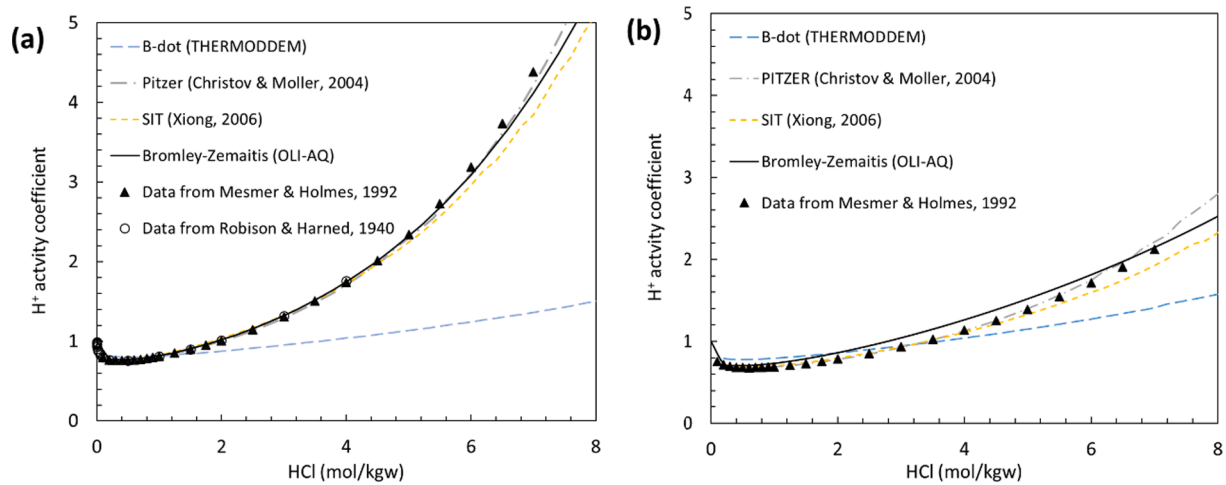


Fig. 2. Evaluation of thermodynamic models for the HCl-H₂O system: comparison of H⁺ activity coefficient calculated with different models and published data (a) at 25 °C and (b) at 100 °C.

2.2.3. Thermodynamic description of the H₂O-HCl-Al-Ca-Si-Na system with SIT interaction parameters

Since no consistent Pitzer model is available for the whole H₂O-HCl-Al-Ca-Si-Na system, a simpler description is required. We chose the Thermoddem database (Blanc et al., 2012) as a starting point to describe all aqueous species of the system. This database includes B-dot model parameters for activity coefficient calculations (see Table 1), and equilibrium constants described in the 25–300 °C temperature range. The database was completed with SIT temperature-dependent interaction parameters for the (Na⁺ Cl⁻), (Ca²⁺ Cl⁻) and (H⁺ Cl⁻) pairs, using the polynomial expressions proposed by Xiong (Xiong, 2006), as well as constant interaction parameters extracted from the Thermochemie database for the (Al³⁺ Cl⁻) pair (Giffaut et al., 2014). All SIT interactions taken into account in our model are compiled in Table 2. It can be noted that no interaction involving Si species is considered in this model, since silica in acid aqueous solutions is predominantly in the form of neutral silicic acid Si(OH)_{4(aq)} (Sjoberg, 1996) while SIT interactions are between ionic species.

The resulting aqueous model was compared to the OLI/AQ model for several configurations, and no major discrepancies were found between the two models. For instance, Fig. 3 displays the activity coefficient of H⁺ and the ionic strength of an aqueous solution composed of 1 kg of water, 200 g of Ca_{0.65}Na_{0.35} anorthosite and up to 250 g of HCl, at 95 °C and 1 atm, calculated with the two models. It should be noted that no solid phase was considered in these calculations in order to specifically evaluate the aqueous phase description. As illustrated in Fig. 3, both models predict an overall increase of $\gamma_{(H^+)}$ from 0.56 without HCl to 1.6–1.8 with 250 g of HCl, while the ionic strength increases from 1.7 to 10.4 mol/kg. The agreement between the two calculations is considered sufficiently good to validate our aqueous model. In addition, we compared the proton activity predicted by PHREEQC/SIT and OLI/AQ

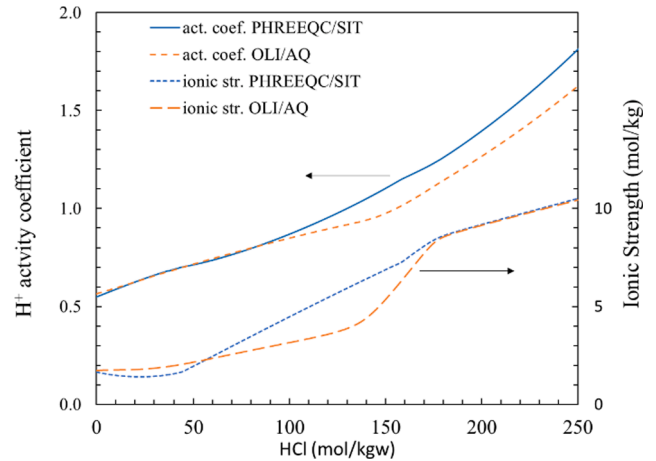


Fig. 3. Evaluation of thermodynamic models for the H₂O-HCl-Al-Ca-Si-Na system: comparison of H⁺ activity coefficient and ionic strength calculated with OLI/AQ and PHREEQC/SIT at 95 °C and 1 atm, in a liquid phase containing 1 kg of water and 200 g of Ca_{0.65}Na_{0.35} anorthosite, without solid phases.

in the conditions used for the kinetic optimization (285 g of Ca_{0.65}Na_{0.35} anorthosite treated by 1250 g of 20 wt% HCl at 105 °C, see § 3.2.4) and both models yielded similar values throughout the dissolution process (see Fig. S1 in the supplementary information).

2.3. Description of the solid phases

In addition to the aqueous phase, solid phases need to be included in the thermodynamic model in order to compute solid-liquid equilibria. Here again, we chose to take into account the solid phases described in the Thermoddem database (Blanc et al., 2012), which includes 128 solid phases containing Na, Ca, Al, Si, Cl elements. Among the solids found to precipitate at equilibrium, quartz was discarded since amorphous silica is more likely to be formed by the precipitation of dissolved silicon (Daval et al., 2011). To make a fair comparison with the AQ database from OLI (which includes 58 solids for the same system), both databases were harmonised. As a result, five solids from Thermoddem, namely heulandite(Ca), beidellite(Ca), gismondine, chabazite, and phillipsite (Na), as well as a solid from OLI/AQ-GE (AlOHCl₂), were set aside.

A comparison of the two models was carried out using the system described earlier (1 kg of water, 200 g of Ca_{0.65}Na_{0.35} anorthosite and up to 250 g of HCl, at 95 °C and 1 atm), including the solid phases. As

Table 2
Compilation of the SIT parameters included in our database.

Pair interaction	Interaction value (T is temperature in K)	Reference
(H ⁺ Cl ⁻)	$0.123 - 1.26 \times 10^{-4} \times (T - 298.15) - 5.39 \times 10^{-7} \times (T - 298.15)^2$	(Xiong, 2006)
(Ca ²⁺ Cl ⁻)	$0.162 + 5.98 \times 10^{-4} \times (T - 298.15) - 1.64 \times 10^{-6} \times (T - 298.15)^2$	(Xiong, 2006)
(Na ⁺ Cl ⁻)	$0.0475 + 5.82 \times 10^{-4} \times (T - 298.15) - 9.54 \times 10^{-7} \times (T - 298.15)^2$	(Xiong, 2006)
(Al ³⁺ Cl ⁻)	0.33	(Giffaut et al., 2014)

illustrated in Fig. 4, the stable solids computed by the two models are slightly different.

The discrepancy between the two models is caused by the slightly different thermodynamic data applied to the main solids of the system. Indeed, as compiled in Table 3, the Gibbs energy of formation of anorthite, low albite and laumontite, exhibits differences greater than 15 kJ/mol between the two databases. Specifically, the low albite phase is much more stable in the AQ-GE database than in the Thermoddem database, which explains why low albite has a large domain of stability in Fig. 4b.

Assessing thermodynamic data is a complicated process which involves the consistency of the whole database. In addition, experimental equilibrium data corresponding to our specific range of conditions were very scarce. Consequently, we chose to keep the thermodynamic data of the Thermoddem database in our model. It can be noted from Fig. 4 that the total amount of HCl required to dissolve all Al-bearing minerals is rather consistent between the two models (about 180 g of HCl for 200 g of anorthosite in 1 kg of water), while the only remaining solid is a pure silica phase.

Finally, we compared our model prediction to data available in the literature (Felmy et al., 1994; Gunnarsson and Arnórsson, 2000) on amorphous silica solubility in NaCl-H₂O at 25 °C and 100 °C (Fig. 5a) and in HCl-H₂O at 23 °C and 47 °C (Fig. 5b). Though these data were the only experimental data of interest that we could find, they are relevant since they are consistent with the conditions found towards the end of dissolution (high chloride concentrations, presence of solid silica). As for the solubility of amorphous silica in water with increasing amounts of NaCl (up to 6 mol/kg), it is very consistent with the model at 25 °C. At 100 °C, there is a discrepancy (about 30%) for intermediate NaCl molalities (1.5 and 2.5 mol/kg), which is reduced at higher molality. As for the HCl-H₂O media, the discrepancies between the model and the data from Felmy et al. (Felmy et al., 1994) are more significant, with an overestimation of the calculated solubility by a factor of about 2. However, there are also significant discrepancies between the data of Gunnarsson and Arnórsson (Gunnarsson and Arnórsson, 2000) and Felmy et al. (Felmy et al., 1994) for low HCl concentrations. Furthermore, it can be highlighted that the temperature dependence is correctly represented in our model (increase of the silica solubility by about 1.5 between 23 °C and 47 °C).

2.4. Parametric study of operating conditions using the selected model

Based on our thermodynamic model, we examined the effect of operating conditions on the leaching of Ca_{0.65}Na_{0.35} anorthosite in HCl-H₂O.

The first parameter concerns the amount of HCl required to leach the phase. The second important parameter is the amount of ore related to the amount of leaching solution (solid-liquid ratio), which varied

between 5 and 25 wt%. For 1 kg of water and a maximal amount of 250 g of acid, this range of solid-liquid ratio corresponds roughly to 65 to 315 g of anorthosite in the system. The four predominance diagrams calculated with our model, showing the speciation of the four main elements (Na, Al, Ca, Si) at 95 °C, are presented in Fig. 6. The diagrams reveal that, regardless of the initial solid-liquid ratio, the leaching of Ca_{0.65}Na_{0.35} anorthosite can lead to the full dissolution of Na, Ca and Al (as Na⁺, Ca²⁺ and Al³⁺ aqueous species), while Si will stay in solid silica. The increase of the initial solid-liquid ratio does not modify any solid-liquid equilibria, but more HCl is required to reach full dissolution.

As for the influence of temperature, it is evidenced in Fig. 7 that this parameter does not play a major role on the solid-liquid equilibria of the system either. Indeed, the model predicts that pyrophyllite (Al₂Si₄O₁₀(OH)₂) is the most stable Al-bearing phase from 20 to 160 °C before aluminium dissolution.

However, the possible occurrence of another ionic species for aluminium above 150 °C – AlH₃SiO₄²⁺ instead of Al³⁺ – can be noted. This aqueous complex should be avoided by restricting the operating temperature to 150 °C since it can possibly immobilize silicon in solution.

As for the thermodynamic study of the leaching of Ca_{0.65}Na_{0.35} anorthosite in HCl-H₂O, we can conclude the following:

- we implemented a thermodynamic model capable of computing solid-liquid equilibria in the H₂O-HCl-Al-Ca-Si-Na multi-element system, with an accurate representation of the activity of H⁺;
- the computing tool (PHREEQC) makes it possible to easily implement kinetics calculations;
- the equilibrium calculations predict that the full dissolution of Na, Ca and Al – as Na⁺, Ca²⁺ and Al³⁺ aqueous species can be achieved while Si will stay in solid silica, in the 20–150 °C temperature range, with a high solid-liquid ratio (up to 25 wt% of minerals in the liquid solution);
- the main limitation of this system is related to the bubble temperature of HCl, which decreases sharply above ~ 20 wt% HCl in water.

The next step of process evaluation is dedicated to the leaching kinetics, which is described in the next section.

3. Kinetic model and best operating conditions for anorthosite acidic dissolution

As explained in the previous section, the PHREEQC tool associated to the SIT-Thermoddem database was chosen to model anorthosite acidic dissolution because of its higher flexibility, and because it was possible to implement conventional ore dissolution models and couple this tool with different numeric computing platforms for parameter estimation.

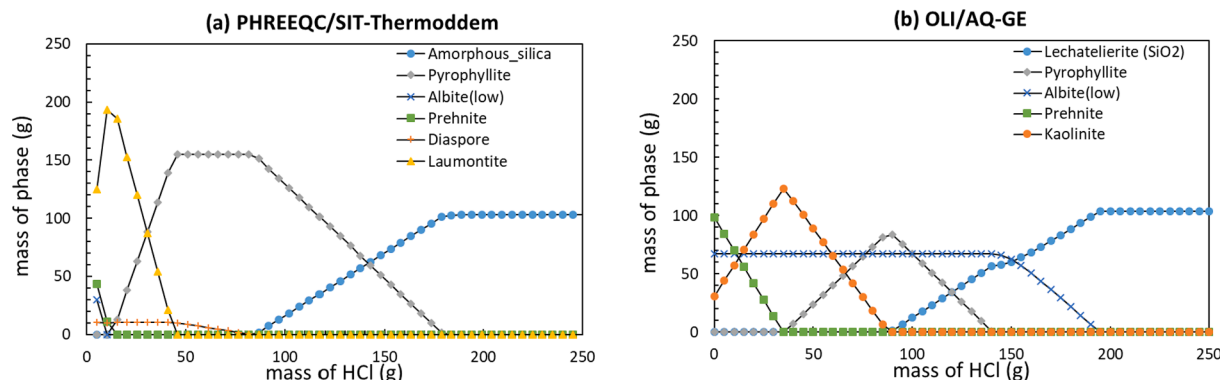
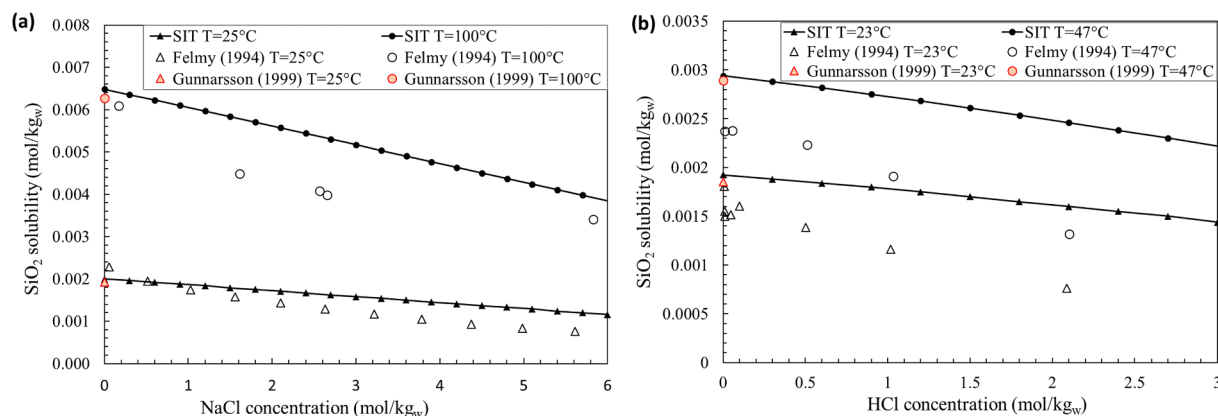


Fig. 4. Stable solid phases resulting from solid-liquid equilibria computed with 200 g of Ca_{0.65}Na_{0.35} anorthosite at 95 °C as a function of the HCl amount added to 1 kg of water: comparison between (a) PHREEQC/SIT-Thermoddem and (b) OLI/AQ-GE.

Table 3Gibbs energy of formation at 298.15 K of the main minerals involved in solid-liquid equilibria for anorthosite leaching in HCl-H₂O.

Mineral name	Chemical formula	Gibbs energy of formation at 298.15 K kJ/mol		Difference(kJ/mol)
		Thermoddem	OLI/AQ-GE	
Anorthite	Ca(Al ₂ Si ₂)O ₈	-4008.3	-3992.7	-15.5
Kaolinite	Al ₂ Si ₂ O ₅ (OH) ₄	-3793.9	-3789.0	-4.9
Albite (low)	NaAlSi ₃ O ₈	-3711.6	-3761.8	50.1
Prehnite	Ca ₂ Al ₂ Si ₃ O ₁₀ (OH) ₂	-5822.6	-5817.9	-4.7
Pyrophyllite	Al ₂ Si ₄ O ₁₀ (OH) ₂	-5266.1	-5255.0	-11.1
Laumontite	Ca(Al ₂ Si ₄)O ₁₂ ·4H ₂ O	-6698.4	-6681.9	-16.4
Amorphous silica/Lechatelierite	SiO ₂	-850.4	-849.0	-1.4
Diaspore	AlO(OH)	-922.7	-913.8	-9.0

**Fig. 5.** Comparison between model calculations and published data for the solubility of amorphous silica at various temperatures, for the systems (a) NaCl-H₂O and (b) HCl-H₂O.

Proton activity $a_{(H^+)}$ being a key parameter of the ore dissolution rate, coupled calculations of thermodynamics and dissolution kinetics are needed to predict the expected performance of the leaching reactor, with respect to process inputs, i.e. temperature, HCl concentration, solid fraction in the feed (and associated PSD).

In this section, we discuss the available information related to anorthosite dissolution mechanisms and kinetics to highlight the major limiting phenomena. A dynamic model is then suggested and implemented with coupled thermodynamic calculations. This model is applied to anorthosite dissolution and assessed with the available quantitative data. The sensitivity analysis of this model towards the major adjustable parameters for ore leaching finally identifies the adequate operating window which should be chosen for the leaching reactor.

3.1. Observations and data from the literature concerning anorthosite acidic dissolution mechanisms

In the 70-80's, the Anortal project, led by IFE, reported interesting tests and observations (Gjelsvik, 1980) on the acid leaching of anorthosite. Patents related to this project (Gaudernack et al., 1978; Gjelsvik and Torgersen, 1983) provide additional quantitative information. One major point lies in the availability of Al atoms in the aluminosilicate framework (Gjelsvik, 1980; Oelkers and Schott, 1995). It appears that Al is more easily extracted from the aluminosilicate framework than Si. Thus, due to the Si/Al ratio of 3 in the alkali feldspar framework (such as albite NaAlSi₃O₈), the removal of Al leaves a partially linked Si tetrahedron. Removal of Si demands the breaking of Si-O bonds, i.e. the decomposition of a Si-rich surface precursor. Therefore, the overall dissolution rate of alkali feldspar is controlled by the decomposition of this precursor, whose formation requests Al removal. However, the anorthite framework (CaAl₂Si₂O₈) has a Si/Al ratio of 1, so the removal of Al leaves a fully detached Si tetrahedron. In this case, it is not

necessary to break Si-O bonds for Si removal. As a consequence, the overall dissolution rate of anorthite is much faster than that of alkali feldspar and it is independent of aqueous Al concentration when conditions are far from equilibrium.

As mentioned earlier, Gjelsvik (Gjelsvik, 1980) thus advised that anorthosite has to contain more than 50 wt% of anorthite to be quantitatively attacked by acid. He reported that alumina extraction depends only on the albite-anorthite ratio, and that impurities or ore crystallinity have a minor impact. His work showed that, when submitted to hydrochloric acid (6 N) in a counter-current column at 105 °C, Gudvangen (Ca_{0.65}Na_{0.35}) anorthosite particles of a few millimetres in size release Al, as well as Na and Ca, while keeping their initial size and shape. Pictures of partially leached particles that were sampled and cut after various contact times clearly show a dark core surrounded by a light residual layer ("ash"), found to be amorphous (as proven through X-ray diffractometry analysis) and thickening in time. Gjelsvik concluded that the dissolution mechanism follows a shrinking core pattern with constant particle size.

On the other hand, experimental data from the same paper, but for finely ground anorthosite, show a strong effect of temperature on acidic leaching in 20 wt% HCl solutions after 2 h (see Fig. 9b). This suggests that the dissolution process obeys chemical reaction control (Levenspiel, 1998). Therefore, a shrinking core model without diffusion limitation in the "ash" layer (equivalent to a shrinking particle model) is suitable to describe the dissolution of sub-millimetric Gudvangen anorthosite in this temperature range.

3.2. Dissolution model for finely ground Gudvangen anorthosite

3.2.1. Shrinking core model with constant particle size and limiting surface reaction

In this work, dissolution of anorthosite particles of various sizes is considered in a perfectly mixed high-concentration HCl aqueous

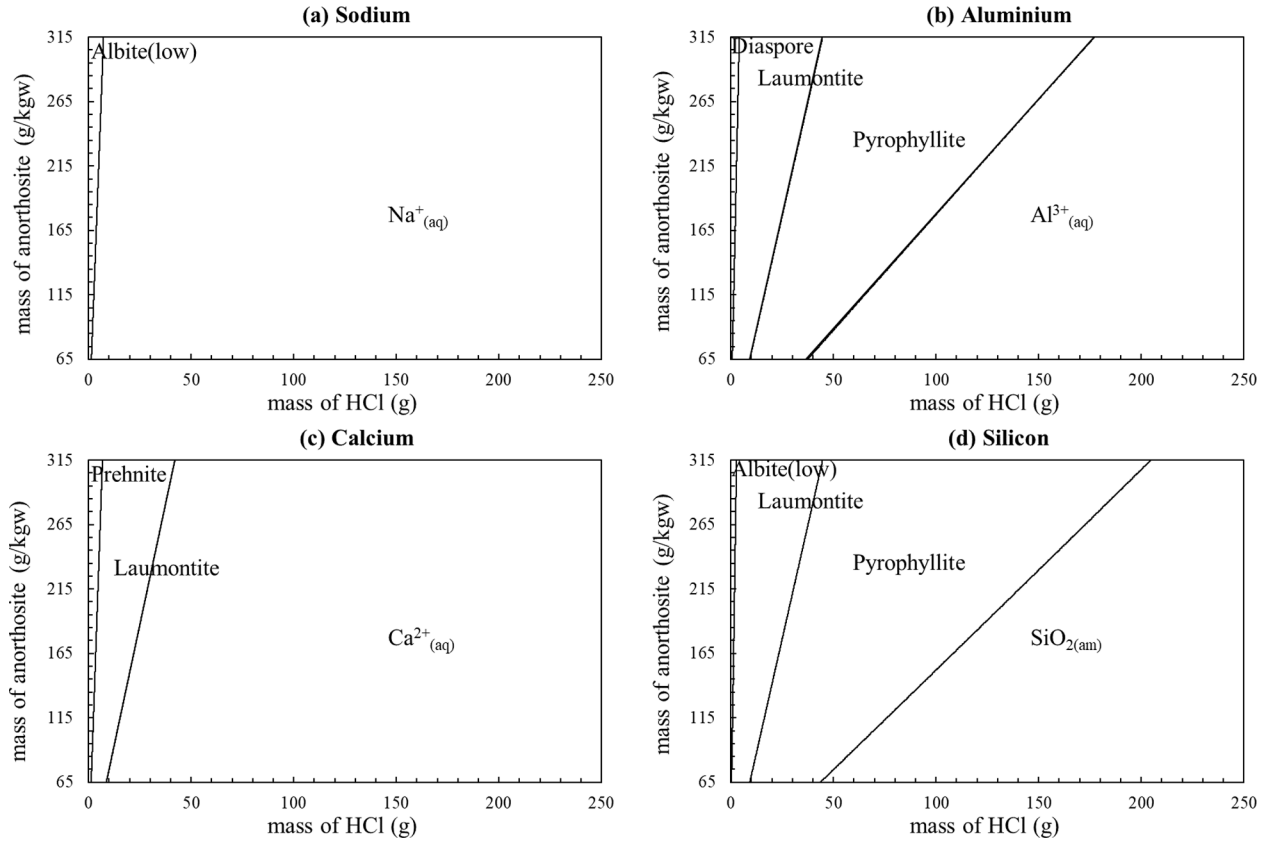


Fig. 6. Influence of anorthosite and hydrochloric acid amounts on the system equilibrium ($T = 95\text{ }^{\circ}\text{C}$; 1 kg of water). Predominance diagrams for (a) Na, (b) Al, (c) Ca, and (d) Si.

solution. The selected operating conditions correspond to those allowing full dissolution of aluminium as Al^{3+} and amorphous silica only as a solid by-product according to the previous thermodynamic predictions: HCl concentration close to the azeotropic composition, S/L ratio < 25 wt % and $T \leq 150\text{ }^{\circ}\text{C}$.

The shrinking core model with constant particle size and control through the surface reaction rate is adopted, in which thermal effects are neglected (uniform and constant temperature) and it is thus considered that no limitation exists for the transport of the dissolved species around the particles and within the porous ash layer.

For each particle, the reactive core is shrinking, but the particle keeps a constant global radius R_{0i} .

The distinct size classes in the particle size distribution (PSD) offer different specific surfaces to the acid attack in the reactor, leading to different lixiviation dynamics. In the present model, a tens of size classes are considered to mimic the actual particle size distribution. In each, the particles are assumed spherical with a smooth surface.

For the selected model, a mass balance applied to the number of moles ' n_i ' of ore in a class 'i' of specific particle size leads to:

$$\frac{dn_i}{dt} = r \cdot \text{SSA}_{0i} \cdot w_{0i} \cdot m_0 \left(\frac{n_i(t)}{n_{0i}} \right)^{2/3} \quad (1)$$

where r is the surface reaction rate ($\text{mol} \cdot \text{m}^{-2} \cdot \text{s}^{-1}$), SSA_{0i} is the specific surface area offered in class i (m^2/g), m_0 the initial ore mass (g), w_{0i} the initial weight fraction for class i , and n_{0i} the initial number of moles of ore in class i .

The surface reaction rate r is modelled through kinetic parameters, i. e. pre-exponential constant, activation energy and reaction order with respect to the activity of reactant (product) ion species (cf. paragraph 3.2.3).

3.2.2. Implementation of the kinetic model using MATLAB and PHREEQC

In the following model, it is considered that PSD obeys a Rosin-Rammler distribution model (Vesilind, 1980), characterized through the d_{90} size and a spread coefficient α . Each class of particle size is then handled as a specific "ore" with corresponding mole number n_i ($1 \leq i \leq N$). For each class i , the core diameter decreases along dissolution. Amorphous silica is prone to be formed by precipitation of dissolved silicon (Daval et al., 2011), but we assume that it does not plug the ash layer around the particles. To compute ore dissolution, the evolution of the PSD of the shrinking cores is described versus time, by means of an algorithm written with the MATLAB® software, whose steps are defined hereafter. The latter is interfaced with PHREEQC, which calculates the liquid and solid speciation at each time step, as well as provides the integration of the kinetic expressions. MATLAB® features then make it possible to optimize the reaction rate parameters from the literature data and to automate the sensitivity analysis with respect to the operating conditions.

The dataset and experimental operating conditions are first uploaded. Then the molar fraction of Ca, Na, Al and Si within the ore are calculated, so as to define the "Phases" module in PHREEQC. For each "ore i " (class i in initial PSD), the interfacial area between liquid and solid phase, the weight percent of 'ore i ' in the whole ore mass, and the mean diameter of "ore i " are calculated and implemented in PHREEQC. The different parts needed in PHREEQC are then separately filled in several blocks: solution definition, equilibrium phases, rate parameters, kinetics. In the kinetics block, the differential mass balance which drives the core shrinking phenomenon (Equation (1)) is set (it should be noted that it uses the reaction rate as specified in the "rate parameters" block), the Runge-Kutta method is selected and the integration step defined. PHREEQC then runs to give the time-integration of the mass balances. At each time-step, the amount of dissolved Al and the new core diameter are computed for each "ore" (size class of PSD), and the new

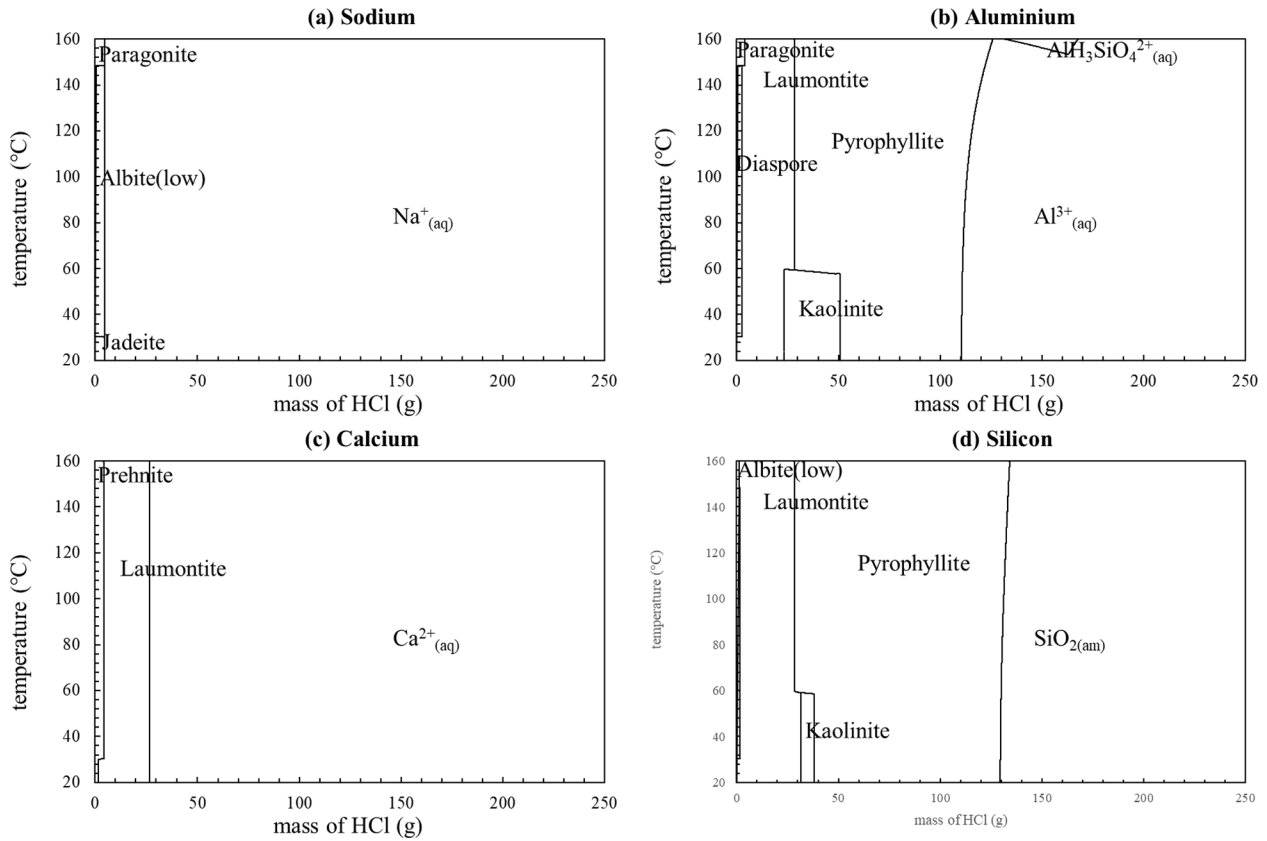


Fig. 7. Influence of temperature and HCl amount on the system equilibrium (200 g of anorthosite; 1 kg of water). Predominance diagrams for (a) Na, (b) Al, (c) Ca, and (d) Si.

composition and species activities are calculated for the liquid solution. The additional amount of precipitated amorphous silica is also deduced.

The computation is stopped when the targeted reaction time is reached. The aluminium extraction yield is deduced from the final amount of dissolved alumina as related to its total initial amount in ore. This calculated yield can then be compared to experimental yields in the literature.

3.2.3. Selection of the surface reaction kinetics for anorthosite acidic dissolution

Several mechanisms have been postulated in the geochemical literature to describe the elementary phenomena in plagioclase dissolution (Oelkers et al., 1994; Oelkers and Schott, 1995; Crundwell, 2014; Gudbrandsson et al., 2014). Oelkers et al. considered the formation of activated complexes by the successive breaking of metal–oxygen bonds in the mineral framework upon proton attack. From their HCl dissolution results of natural Fuggoppe anorthite in a stirred reactor ($2.4 < \text{pH} < 3.1$; $45^\circ\text{C} < T < 95^\circ\text{C}$), they suggested that the metal-proton exchange reactions lead to completely detached Si tetrahedra, and thus that the hydrolysis of the Si-O bond is unnecessary (Oelkers and Schott, 1995). According to this elementary mechanism, Oelkers et al. stated that the anorthite dissolution rate, when conditions are far from equilibrium, is a function of proton activity only. They derived the following dissolution rate from their experiments:

$$r = k \cdot a_{(\text{H}^+)}^{3/\eta} \quad (2)$$

where $a_{(\text{H}^+)}$ is the activity of protons and η designates the number of precursor complexes formed by the adsorption of three protons.

For albite on the other hand, the same authors stated that the dissolution rate also depends on the aqueous aluminium concentration (with r function of $a_{(\text{H}^+)}/(a_{(\text{Al}^{3+})})^{1/3}$), since in this case the dissolution is controlled by the relatively slow destruction of Si-O-Si bonds in the Al-

deficient and Si-rich precursor complex (Oelkers et al., 1994).

In contrast, Crundwell (Crundwell, 2014) considered an independent reaction of metal atoms and silicate groups. Their model predicts feldspar dissolution rate to be one-half order in H^+ .

All these approaches lead to the following generic expression for the surface reaction rate:

$$r = k_0 \cdot \exp(-E_a/(RT)) \cdot a_{(\text{H}^+)}^n \cdot a_{(\text{Al}^{3+})}^m \cdot (1-10^{\text{SI}/\sigma}) \quad (3)$$

with $n > 0$, $m \leq 0$, $\sigma > 0$ (typically $\sigma = 1$) and where k_0 is the pre-exponential constant, E_a the activation energy, a the activity of the species, and SI the saturation index.

The values of these reaction rate parameters are available in different studies (Palandri and Kharaka, 2004; Declercq and Oelkers, 2014) for labradorite or for bytownite ($\text{Ca}_x\text{Na}_{1-x}$ anorthosites with $x = 0.5-0.7$ or $x = 0.7-0.9$, respectively). However, the resulting reaction rates can differ by several orders of magnitude in the temperature range of interest, since they are strongly dependent on the bulk ore composition (Ca/Na content) and mineral alteration (Velduyzen, 1995; Wanvik, 2000). This underlines the need of a specific parameter estimation for the investigated ore.

3.2.4. Application to the Anortal project data

The reaction rate parameters therefore had to be optimized on the basis of dissolution experiments with known conditions and ore properties, since the reaction rate values found in the literature exhibit large discrepancies. The extraction yields given by Gjelsvik (Gjelsvik, 1980) as a function of dissolution time and reaction temperature were used as the reference data for assessment. They correspond to a finely ground Gudvangen ($\text{Ca}_{0.65}\text{Na}_{0.35}$) anorthosite treated with a 20 wt% HCl solution in a stirred tank. The exact PSD of the ore was not given, nor the solid to liquid ratio, but the NGU Report (Wanvik, 2010) indicates likely values of 50–75 μm and 23%, respectively. As such, for the solid phase,

either a single size class of 65 μm , or a d_{90} of 75 μm with a mean Rosin-Rammler diameter of 50 μm ($\alpha = 2$), were assumed.

An optimization algorithm was built to identify the most relevant values for the surface reaction rate. In the model, the reaction order with respect to $a_{(\text{H}^+)}$ was set to the value suggested in Palandri and Kharaka (Palandri and Kharaka, 2004) for labradorite ($n = 0.626$ in Equation 3) since HCl concentration did not vary and the literature usually agrees on a “ n ” value close to 0.5 (Crundwell, 2014). Possible inhibitory effect of $a_{(\text{Al}^{3+})}$ was also neglected ($m = 0$ in Equation 3).

As mentioned before, the precipitation of silica was assumed to be instantaneous, without hindering ore dissolution. Initial values of pre-exponential constant and activation energy were taken from Palandri and Kharaka as well.

Leaching of $\text{Ca}_{0.65}\text{Na}_{0.35}$ anorthosite at various temperatures was computed for each size class as described in paragraph 3.2.1, considering an overall initial ore mass of 285 g treated in 1250 g of 20 wt% HCl solution. For that purpose, the PHREEQC dissolution script was embedded into a MATLAB program to be coupled with the optimization toolbox for parameter fitting. The sum of squared residuals between the corresponding extraction yields and the experimental yields was calculated for the whole available dataset (cf. Fig. 9). Then, the *fminsearch* routine (based on the Nelder-Mead simplex method) determined the optimal reaction rate parameters for its minimization.

The modification of the size distribution of the reactive cores can be observed, as illustrated in Fig. 8 in the case of 16 classes of $\text{Ca}_{0.65}\text{Na}_{0.35}$ anorthosite being leached at 105 $^{\circ}\text{C}$ and modelled following the optimized kinetic law.

The data fitting gives satisfactory results as shown in Fig. 9. The best fit was obtained when accounting for particle size dispersion rather than a single size class, but both investigated cases essentially gave the same order of magnitude for the reaction rate parameters. The values corresponding to the best fit are as followed: $k_{(\text{T} = 105^{\circ}\text{C})} = 1.03 \cdot 10^{-9} \text{ mol.cm}^{-2} \cdot \text{s}^{-1}$ and $E_a = 65.9 \text{ kJ/mol}$. This activation energy is very similar to the value given in the JNC Tokai Works report (Arthur et al., 2000) for labradorite ($E_a = 65 \text{ kJ/mol}$).

On the other hand, the calculated value of $k_{(\text{T} = 105^{\circ}\text{C})}$ is significantly higher than the values inferred from Palandri and Kharaka (Palandri and Kharaka, 2004) or from the JNC Tokai Works report ($5 \cdot 10^{-11}$ and $3.6 \cdot 10^{-11} \text{ mol.cm}^{-2} \cdot \text{s}^{-1}$, respectively). It remains however below the one obtained for bytownite by these authors ($1.7 \cdot 10^{-9} \text{ mol.cm}^{-2} \cdot \text{s}^{-1}$), in agreement with an increase of anorthosite reactivity with Ca content.

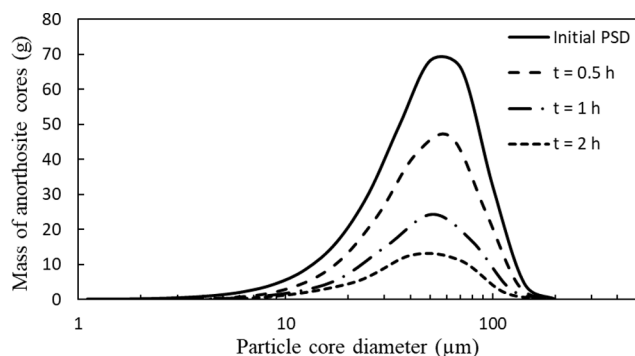


Fig. 8. Time-evolution of core size distribution for $\text{Ca}_{0.65}\text{Na}_{0.35}$ anorthosite ($285 \text{ g}_{\text{ore}}/\text{kg}_{\text{water}}$) leached at 105 $^{\circ}\text{C}$ in a 20 wt% HCl solution. Initial PSD obeys a Rosin-Rammler distribution model with $d_{90} = 75 \mu\text{m}$ and $\alpha = 2$. Computed results are obtained for the optimized surface reaction rate law with $n = 0.626$, $k_{(\text{T} = 105^{\circ}\text{C})} = 1.03 \cdot 10^{-9} \text{ mol.cm}^{-2} \cdot \text{s}^{-1}$ and $E_a = 65.9 \text{ kJ/mol}$.

3.3. Sensitivity analysis of alumina extraction to operating parameters, and identification of a suitable operating window for the industrial lixiviation reactor

The optimized model was then applied to predict the performance of the batch dissolution reactor with respect to the process inputs. The S/L ratio was kept to 23 wt%, close to the maximum value ensuring that amorphous silica is the only solid phase (cf. Fig. 6).

Fig. 10 gives an example of the effects of temperature and ore PSD (modifying the d_{90} at fixed spread coefficient) on the time-extraction yield of aluminium. Note that the hypothesis of surface reaction control was supposed to remain valid over this extended range of conditions, since the proposed model lead to extraction yields close to those reported in the patent of Aranda and Mastin (Aranda and Mastin, 2015) for a temperature of 140 $^{\circ}\text{C}$ and a particle size of 300 μm (see Fig. S2 in supplementary information).

Temperature appears to be one of the main process levers due to the relatively high apparent energy activation under chemical reaction control. However, it is worth recalling that the boiling point of the 20 wt % HCl solution is 108 $^{\circ}\text{C}$, meaning that above this temperature, it needs to be placed under pressure. Increasing the mean particle size of the ore decreases the overall anorthosite dissolution rate due to a lower specific area of the particles. Nonetheless, extraction yields as high as 90% can still be achieved after 3 h, when processing sub-millimetre particles at 150 $^{\circ}\text{C}$. A full techno-economical assessment would be needed to further refine the choice of the optimal operating conditions by considering for instance the costs of heating and grinding. However, it can already be pointed out that the process cost will be also determined by the reachable silica purity, accounting for its probable precipitation onto the original particles, and by the complexity of its filtration.

Dried precipitated synthetic amorphous silica (as used in rubber, paints and coating) typically contains $\geq 95 \text{ wt\% SiO}_2$ (Rompp, 1998), while a minimum value of 85 wt% is set in almost all national standards for its application as supplementary cementitious materials (Cement Concrete & Aggregates Australia, 2018). The solid product could then be directly used in cement raw meal, as a substitute for a portion of primary raw materials, lowering the requirements for silica to alumina ratio.

To fulfil the most stringent examples of aforementioned silica specifications while operating the leaching within a reasonable reaction time (a couple of hours), temperatures above 110 $^{\circ}\text{C}$ and ore particle diameter below 500 μm should be privileged, as shown in Fig. 11. Note that these curves are based on the speciation obtained at the reaction temperature, while significantly increased amounts of silicon in solution are found when the temperature is raised above 100 $^{\circ}\text{C}$. Therefore, the time needed to reach the targeted values of purity could be reduced if a cooling step after leaching is accounted for (resulting in an increase of the amount of precipitated SiO_2).

On the other hand, in their patent, Gjelsvik and Torgersen recommended (Gjelsvik and Torgersen, 1983) the use of anorthosite particles with about 90% of the grains having a minimum diameter of 100 μm to ease the separation of precipitated silica by classical vacuum filters, as used for high tonnage materials with a moderate added value. This would then typically correspond to the PSD with d_{90} value of 412.5 μm previously considered.

4. Toward the design of a continuous process

During the leaching process in a batch reactor, the dissolution of the ore slows down due to (i) the reduction of the active surface, as well as (ii) the acid consumption that results in lowering the activity of the proton. On the opposite, a continuous stirred tank reactor (CSTR) operates at the residual acid concentration corresponding to the final ore conversion.

Therefore, to mimic the performance of the batch process, a series of stirred tanks should be applied (see Fig. 12). Moreover, operating counter-current leaching (with opposite flow of solid and solution) may

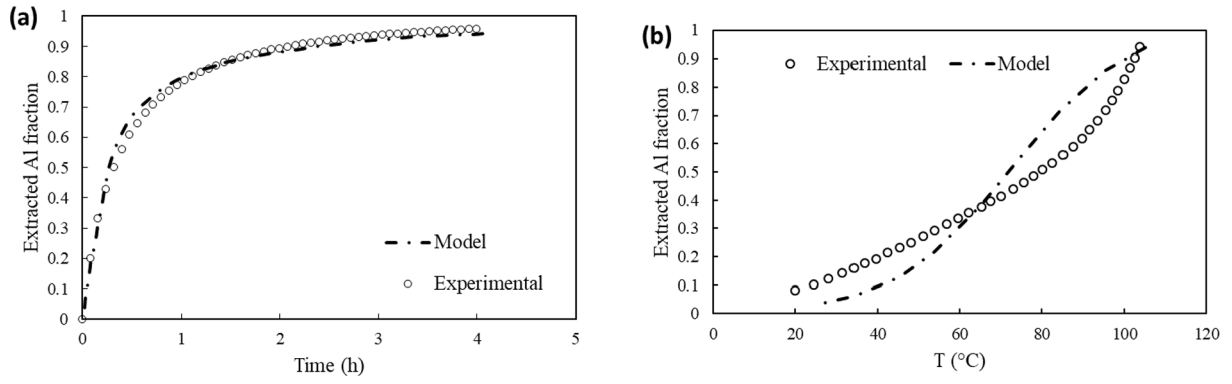


Fig. 9. Experimental and predicted aluminium extraction yields (a) as a function of time at 105 °C and (b) as function of temperature after 2 h of reaction, for finely ground $\text{Ca}_{0.65}\text{Na}_{0.35}$ anorthosite ($d_{90} = 75 \mu\text{m}$) treated with a 20 wt% HCl solution (experimental data from Gjelsvik (Gjelsvik, 1980)).

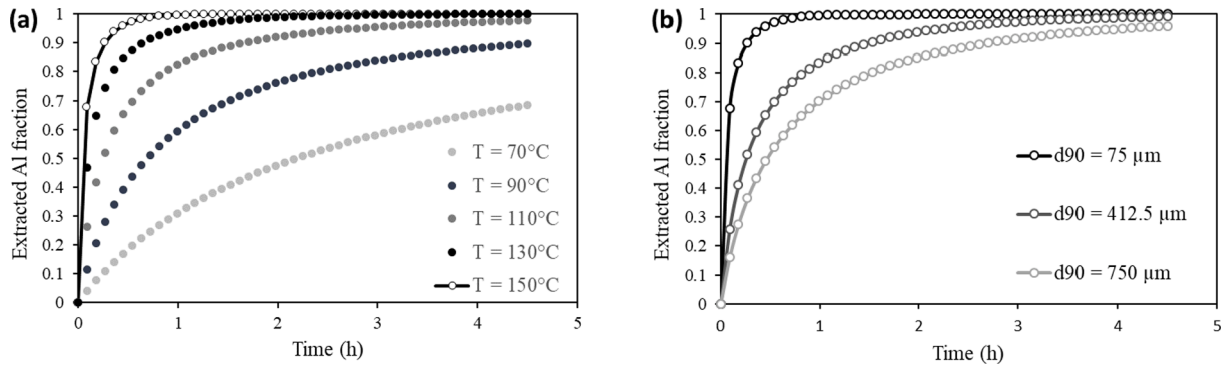


Fig. 10. Effects of (a) temperature ($d_{90} = 75 \mu\text{m}$) and (b) d_{90} value of the ore PSD ($T = 150 \text{ }^\circ\text{C}$) on the time-extraction yield of aluminium for $\text{Ca}_{0.65}\text{Na}_{0.35}$ anorthosite treated by 20 wt% HCl solution ($S/L = 23 \text{ wt}\%$).

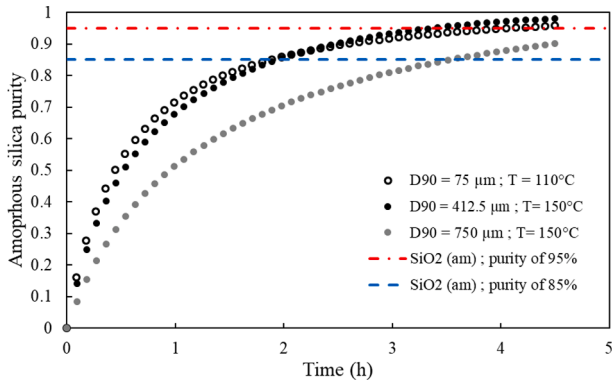


Fig. 11. Effects of temperature and ore PSD on the reaction time needed to reach targeted values of amorphous silica purity (respectively, 85% and 95%) for $\text{Ca}_{0.65}\text{Na}_{0.35}$ anorthosite treated with a 20 wt% HCl solution ($S/L = 23 \text{ wt}\%$).

further enhance the extraction yields by contacting the exhausted ore with the fresh acid solution (Haque et al., 1987).

In order to gain knowledge about the batch-to-continuous processing of the targeted ore, the extraction yields were evaluated for several continuous reactor configurations, using the optimized kinetic expression evaluated in paragraph 3.2.4. Based on a segregated-flow approach (where the solid behaves as a macrofluid), the conversion extent $X_{\text{ore,out}}$ of a monodisperse ore in the continuous leaching reactor can be deduced from the following expression (Levenspiel, 1998):

$$1 - X_{\text{ore,out}} = \int_0^{\infty} (1 - X_{(t,R_0,C_{H^+})}) E_{S(t,R_0)} dt \quad (4)$$

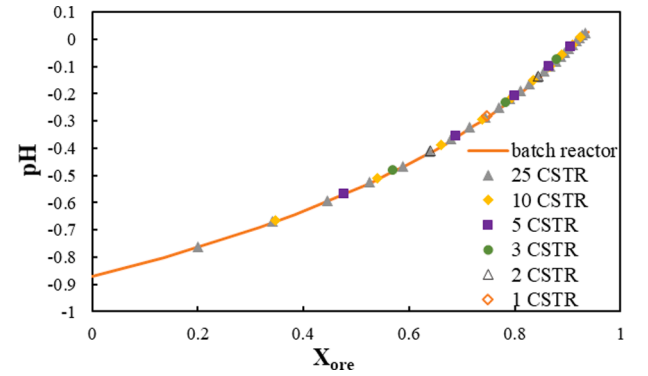


Fig. 12. Evolution of solution pH vs. the overall molar dissolution extent of anorthosite ($T = 150 \text{ }^\circ\text{C}$, feed acid concentration = 20 wt% HCl, $S/L = 23 \text{ wt}\%$, polydisperse ore with $d_{90} = 412.5 \mu\text{m}$): solid line is for the batch operation, and symbols for the outlet of CSTR in series operating with co-current flow of solution and solid.

where $X_{(t,R_0,C_{H^+})}$ is the conversion extent of the ore in batch conditions (function of the reaction time t , the initial radius of the ore particle R_0 and the acid concentration C_{H^+}), t_0 the required time for the complete conversion of the ore particle of radius R_0 , and $E_{S(t,R_0)}$ the residence time distribution of the solid in the reactor.

In the case of a perfectly mixed tank and a particle dissolution under chemical reaction control, Equation (4) becomes:

$$X_{\text{ore,out}} = \frac{3\tau_S}{t_0} \left(6 \left(\frac{\tau_S}{t_0} \right)^2 + 6 \left(\frac{\tau_S}{t_0} \right)^3 \left(1 - \exp \left(- \frac{t_0}{\tau_S} \right) \right) \right) \quad (5)$$

with τ_s the mean residence time of the solid and t_0 given by the surface reaction rate, according to:

$$t_0 = \frac{\rho_{m,ore,0} R_0}{k_0 \exp\left(-\frac{E_A}{RT}\right) a_{H^+out}^n} \quad (6)$$

($\rho_{m,ore,0}$ being the molar density of the initial ore (mol/m³)).

Equation (5) was generalized to polydisperse particles by adding the weighted contributions of each size class, supposing that they all exhibited the same residence time distribution (Levenspiel, 1998). It is worth mentioning that the mean conversion extent at the reactor outlet could have been alternatively evaluated in a single step using the Multiple Convolution Integral method proposed by Dixon (Dixon, 1996).

To solve Equation (5), the value of the activity of the proton inside the CSTR is needed, which itself depends on the actual ore conversion as per the stoichiometry. Given $X_{ore,out}$, $a_{H^+out}^n$ can be obtained from an equilibrium calculation using PHREEQC where only the amount of ore to be converted is put into contact with the acid solution. An iterative procedure was thus performed until convergence of $X_{ore,out}$, using the optimization routine *fminsearch* from MATLAB®.

For reactors in series with co-current flow of solid and solution, the same procedure could be successively applied to each reactor after updating the PSD of the active cores and the solution composition between each.

In the case of counter-current leaching, the successive conversion extents in the reactor series had to be optimized altogether. They were initialized using the values obtained in the co-current configuration. The optimization routine *fmincon* of MATLAB® was then applied with inequality constraints for the consecutive values of $X_{ore,out}$ in the series. An ideal liquid/solid separation was also assumed at each reactor outlet.

These calculations were exemplified for the conditions previously highlighted: a processed ore with a d_{90} value of 412.5 μm and a reaction temperature of 150 °C. Fig. 13a shows as expected a lowered extraction performance when switching from the batch reactor to the single CSTR, while the system of 10 mixed tanks in series with co-current flow closely approaches the performance of the former. On the other hand, Fig. 13b underlines the fact that the counter-current process can outperform the batch performance when using 5 CSTR only.

In this case, such behaviour is only the result of the complex interplay between ore conversion and pH evolution. A more efficient use of acid in counter-current operation for anorthosite dissolution has been confirmed experimentally by Bremner et al. (Bremner et al., 1982).

5. Conclusions and perspectives

The proposed work was designed to (i) develop a theoretical investigation of anorthosite leaching in HCl media, (ii) to account for the

complexity of the electrolyte solution, (iii) to predict the variety of solid by-products that could form and finally, (iv) to give a reliable description of the process kinetics for an ore composition that could fulfil the requirement of quantitative aluminium extraction.

Several learnings were drawn from this study:

- Regarding thermodynamic modelling, we showed that the SIT model, which requires a limited number of empirical parameters, is able to represent the complex aqueous solution in the typical operating conditions with HCl concentration up to the azeotrope composition. The model computes acceptable values for proton activity, which is a key parameter to calculate the surface reaction rate. The two geochemical databases applied predict essentially the formation of the same solid phases, though some differences are found in regard to their stability, as for example in the case of albite.
- A first operating window was thus established, in which amorphous silica is selectively precipitated, while the other constituting elements of anorthosite are leached in the aqueous solution. It mainly depends on the concentration of the HCl solution used and the ore concentration, restricting the S/L ratio to ca. 25 wt% for the azeotropic HCl solution. On the other hand, temperature has only a minor effect on the solid phase speciation.
- Based on available experimental data, we built a kinetic model accounting for the dissolution rate of anorthosite, taking into account the effect of temperature, the amount and particle size distribution of the solid phase, and the concentration of HCl. We showed that temperature strongly affects the dissolution rate of Gudvangen anorthosite, due to a high apparent activation energy, in line with a process mainly driven by surface reaction. Particle size distribution of the ore particles also significantly influences the time-extraction yield, and grain size should be kept below the millimetre range to result, within a few hours, in an extensive ore dissolution, as required by silica purity standards.
- Given the effect of acid consumption on the reaction rate for the concentrated slurry, counter-current leaching could be profitable to increase aluminium extraction yield and silica purity.

In the context of the European AlSiCal project, the trends and conclusions derived from this model will be confronted to an extensive experimental database obtained by varying the pivotal process parameters. The physico-chemical characterization of the solid products will also make it possible to refine the model hypotheses pertaining to the dissolution mechanism. Finally, this modelling approach can also be extended to other alternative sources of aluminium examined in the project.

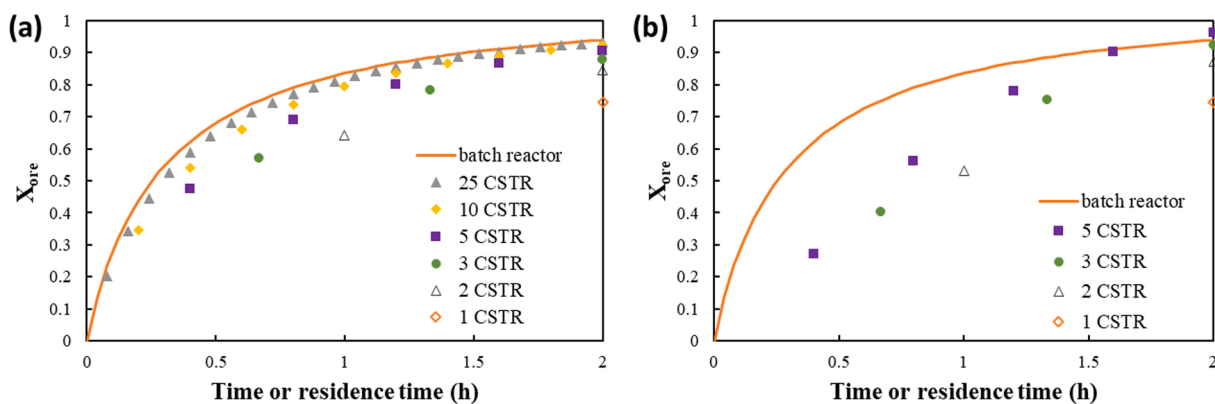


Fig. 13. Evolution of the conversion extent of anorthosite as a function of the reaction time (batch reactor) or mean residence time (continuous process) for a series of CSTR operating (a) with co-current flow of solid and liquid, and (b) with counter-current flow ($T = 150\text{ °C}$, feed acid concentration = 20 wt% HCl, S/L = 23 wt%, total residence time = 2 h, polydisperse ore with $d_{90} = 412.5\text{ }\mu\text{m}$).

CRediT authorship contribution statement

Thomas Neron: Methodology, Software, Investigation, Writing – original draft, Visualization. **Laurent Cassayre:** Conceptualization, Methodology, Investigation, Writing – original draft, Writing – review & editing. **Xuan Zhuo:** Software, Investigation. **Marie-Hélène Manero:** Writing – original draft. **Florent Bourgeois:** Writing – review & editing. **Anne-Marie Billet:** Writing – original draft, Investigation, Supervision. **Carine Julcour:** Conceptualization, Methodology, Software, Investigation, Writing – original draft, Writing – review & editing, Supervision, Project administration.

Declaration of Competing Interest

The authors declare that they have no known competing financial interests or personal relationships that could have appeared to influence the work reported in this paper.

Acknowledgments

This study was supported by the European Union's Horizon 2020 research and innovation programme under grant agreement No 820911, project AlSiCal – Towards a greener mineral and metal industry in Europe (project led by the Institute for Energy Technology, Norway). The authors wish to thank the project partners for the fruitful discussions on the modelling of the dissolution reactor.

Appendix A. Supplementary data

Supplementary data to this article can be found online at <https://doi.org/10.1016/j.mineng.2022.107500>.

References

- Andrako, A., Wang, P., Rafal, M., 2002. Electrolyte solutions: from thermodynamic and transport property models to the simulation of industrial processes. Fluid Phase Equilibria, Proceedings of the Ninth International Conference on Properties and Phase Equilibria for Product and Process Design 194–197, 123–142. [https://doi.org/10.1016/S0378-3812\(01\)00645-8](https://doi.org/10.1016/S0378-3812(01)00645-8).
- Aranda, A., Mastin, J., 2015. Alumina and carbonate production method from al-rich materials with integrated CO₂ utilization. WO2015137823A1.
- Arthur, R.C., Savage, D., Sasamoto, H., Shibata, M., Yui, M., 2000. Compilation of kinetic data for geochemical calculations (No. JNC-TN-8400-2000-005). Japan Nuclear Cycle Development Inst.
- Bayer, 1894. Process of obtaining alumina. US515895A.
- Bayer, 1888. Process of obtaining alumina. US382505A.
- Blanc, P.H., Lassin, A., Piantone, P., Azaroual, M., Jacquemet, N., Fabbri, A., Gaucher, E. C., 2012. Thermodem: A geochemical database focused on low temperature water/rock interactions and waste materials. Appl. Geochem. 27 (10), 2107–2116. <https://doi.org/10.1016/j.apgeochem.2012.06.002>.
- Braaten, O., 1991. The Anortol project in retrospect. Presented at the Ketil Motzfeldt Symposium, The Norwegian Institute of Technology, University of Trondheim, Norway, pp. 175–198.
- Bremner, P.R., Eisele, J.A., Bauer, D.J., 1982. Aluminum extraction from anorthosite by leaching with hydrochloric acid and fluoride, Report of investigations. U.S. Dept. of the Interior, Bureau of Mines, Pgh., Pa.
- Bromley, L.A., 1973. Thermodynamic properties of strong electrolytes in aqueous solutions. AIChE J. 19 (2), 313–320. <https://doi.org/10.1002/aic.690190216>.
- Cement Concrete & Aggregates Australia, 2018. Amorphous Silica Properties, Characterisation and Uses.
- Christov, C., Moller, N., 2004. Chemical equilibrium model of solution behavior and solubility in the H-Na-K-OH-Cl-HSO₄-SO₄-H₂O system to high concentration and temperature. Associate editor: D. J. Wesolowski. Geochimica et Cosmochimica Acta 68 (6), 1309–1331. <https://doi.org/10.1016/j.gca.2003.08.017>.
- Crundwell, F.K., 2014. The mechanism of dissolution of minerals in acidic and alkaline solutions: Part II Application of a new theory to silicates, aluminosilicates and quartz. Hydrometallurgy 149, 265–275. <https://doi.org/10.1016/j.hydromet.2014.07.003>.
- Daval, D., Sissmann, O., Menguy, N., Saldi, G.D., Guyot, F., Martinez, I., Corvisier, J., Garcia, B., Machouk, I., Knauss, K.G., Hellmann, R., 2011. Influence of amorphous silica layer formation on the dissolution rate of olivine at 90°C and elevated pCO₂. Chem. Geol. 284 (1–2), 193–209. <https://doi.org/10.1016/j.chemgeo.2011.02.021>.
- Declercq, J., Oelkers, E.H., 2014. CarbFix Report: PHREEQC Mineral Dissolution Kinetics Database.
- Dixon, D.G., 1996. The multiple convolution integral: A new method for modeling multistage continuous leaching reactors. Chem. Eng. Sci. 51 (21), 4759–4767. [https://doi.org/10.1016/0009-2509\(96\)00334-X](https://doi.org/10.1016/0009-2509(96)00334-X).
- European Economic and Social Committee, 2020. Résilience des matières premières critiques: la voie à suivre pour un renforcement de la sécurité et de la durabilité [WWW Document]. European Economic and Social Committee. URL <https://www.eesc.europa.eu/fr/our-work/opinions-information-reports/opinions/resilience-des-matieres-premieres-critiques-la-voie-suivre-pour-un-renforcement-de-la-securite-et-de-la-durabilite> (accessed 6.9.21).
- Felmy, A.R., Schroeder, C.C., Mason, M.J., 1994. A solubility model for amorphous silica in concentrated electrolytes (No. PNL-SA-25345; CONF-940813-33). Pacific Northwest Lab., Richland, WA (United States). <https://doi.org/10.2172/10110157>.
- Gaudernack, B., Gjelsvik, N., Farbu, L., 1978. Process for the extraction of alumina from aluminum-containing silicates. US4110399A.
- Giffaut, E., Grivé, M., Blanc, P.H., Vieillard, P.H., Colàs, E., Gailhanou, H., Gaboreau, S., Marty, N., Madé, B., Duro, L., 2014. Andra thermodynamic database for performance assessment: ThermoChimie. Applied Geochemistry, Geochemistry for Risk Assessment: Hazardous waste in the Geosphere 49, 225–236. <https://doi.org/10.1016/j.apgeochem.2014.05.007>.
- Gjelsvik, 1980. Extracting alumina from soluble anorthosite by the Anorthal process. Light metals, Proceedings of the 109th AIME Annual Meeting in Las Vegas, Nevada, 133–148. American Institute of Mining, Metallurgical, and Petroleum Engineers, New York.
- Gjelsvik, N., Torgersen, J.H., 1983. Method of acid leaching of silicates. US4367215A.
- Gudbrandsson, S., Wolff-Boenisch, D., Gislason, S.R., Oelkers, E.H., 2014. Experimental determination of plagioclase dissolution rates as a function of its composition and pH at 22°C. Geochim. Cosmochim. Acta 139, 154–172. <https://doi.org/10.1016/j.gca.2014.04.028>.
- Gunnarsson, I., Arnórsson, S., 2000. Amorphous silica solubility and the thermodynamic properties of H₄SiO₄ in the range of 0° to 350°C at Psat. Geochim. Cosmochim. Acta 64 (13), 2295–2307. [https://doi.org/10.1016/S0016-7037\(99\)00426-3](https://doi.org/10.1016/S0016-7037(99)00426-3).
- Haque, K.E., Laliberté, J.J., Pruneau, J., 1987. Batch and counter-current acid leaching of uranium ore. Hydrometallurgy 17 (2), 229–238. [https://doi.org/10.1016/0304-386X\(87\)90054-5](https://doi.org/10.1016/0304-386X(87)90054-5).
- Herz, N., 1969. Anorthosite belts, continental drift, and the anorthosite event. Science 164 (3882), 944–947.
- Julcour, C., Cassayre, L., Benhamed, I., Diouani, J., Bourgeois, F., 2020. Insights Into Nickel Slag Carbonation in a Stirred Bead Mill. Front. Chem. Eng. 2 <https://doi.org/10.3389/fceng.2020.588579>.
- Kaußen, F.M., Friedrich, B., 2018. Phase characterization and thermochemical simulation of (landfilled) bauxite residue (“red mud”) in different alkaline processes optimized for aluminum recovery. Hydrometallurgy 176, 49–61. <https://doi.org/10.1016/j.hydromet.2018.01.006>.
- Levenspiel, O., 1998. Chemical Reaction Engineering, 3rd. Edition by Octave Levenspiel.
- May, P.M., Rowland, D., 2017. Thermodynamic Modeling of Aqueous Electrolyte Systems: Current Status. J. Chem. Eng. Data 62 (9), 2481–2495. <https://doi.org/10.1021/acs.jced.6b01055>.
- Mayer, W.M., Burke, I.T., Gomes, H.I., Anton, Á.D., Molnár, M., Feigl, V., Ujaczki, É., 2016. Advances in Understanding Environmental Risks of Red Mud After the Ajka Spill. Hungary. J. Sustain. Metall. 2 (4), 332–343. <https://doi.org/10.1007/s40831-016-0050-z>.
- Mesmer, R.E., Holmes, H.F., 1992. pH, Definition and measurement at high temperatures. J. Solution Chem. 21 (8), 725–744. <https://doi.org/10.1007/BF00651506>.
- Mihajlović, I., Đurić, I., Živković, Ž., 2014. ANFIS based prediction of the aluminum extraction from boehmite bauxite in the Bayer process. Polish J. Chem. Technol. 16 (1), 103–109. <https://doi.org/10.2478/pjct-2014-0018>.
- Oelkers, E.H., Schott, J., 1995. Experimental study of anorthite dissolution and the relative mechanism of feldspar hydrolysis. Geochim. Cosmochim. Acta 59 (24), 5039–5053. [https://doi.org/10.1016/0016-7037\(95\)00326-6](https://doi.org/10.1016/0016-7037(95)00326-6).
- Oelkers, E.H., Schott, J., Devidal, J.-L., 1994. The effect of aluminum, pH, and chemical affinity on the rates of aluminosilicate dissolution reactions. Geochim. Cosmochim. Acta 58 (9), 2011–2024. [https://doi.org/10.1016/0016-7037\(94\)90281-X](https://doi.org/10.1016/0016-7037(94)90281-X).
- Palandri, J.L., Kharaka, Y.K., 2004. A compilation of rate parameters of water-mineral interaction kinetics for application to geochemical modeling [WWW Document]. URL <https://pubs.usgs.gov/of/2004/1068/> (accessed 6.9.21).
- Parkhurst, D.L., Appelo, C.A.J., 2013. Description of input and examples for PHREEQC version 3: a computer program for speciation, batch-reaction, one-dimensional transport, and inverse geochemical calculations (USGS Numbered Series No. 6-A43), Techniques and Methods. U.S. Geological Survey, Reston, VA.
- Robinson, R.A., Harned, H.S., 1941. Some Aspects of the Thermodynamics of Strong Electrolytes from Electromotive Force and Vapor Pressure Measurements. Chem. Rev. 28 (3), 419–476.
- Rompp, H., 1998. Rompp Lexikon, Lacke und Druckfarben Gebundene Ausgabe.
- Saravi, S.H., Honarparvar, S., Chen, C.-C., 2018. Thermodynamic modeling of HCl-H₂O binary system with symmetric electrolyte NRTL model. J. Chem. Thermodyn. 125, 159–171. <https://doi.org/10.1016/j.jct.2018.05.024>.
- Sjoberg, S., 1996. Silica in aqueous environments. J. Non-Cryst. Solids 196, 51–57. [https://doi.org/10.1016/0022-3093\(95\)00562-5](https://doi.org/10.1016/0022-3093(95)00562-5).
- USGS, 2020. USGS Online Publications Directory [WWW Document]. URL <https://pubs.usgs.gov/periodicals/mcs2020/> (accessed 6.9.21).
- Velduyzen, H., 1995. Aluminium Extraction from an Ontario Calcic Anorthosite by Acid Processes and Resultant Products-Aluminium Chemicals, Coatings, Fillers, Absorbent and Cement Additive (ONTARIO GEOLOGICAL SURVEY No. 5919).
- Vesilind, P.A., 1980. The Rosin-Rammler particle size distribution. Resour. Recovery Conserv. 5 (3), 275–277. [https://doi.org/10.1016/0304-3967\(80\)90007-4](https://doi.org/10.1016/0304-3967(80)90007-4).

- Vidal, O., Rostom, F., François, C., Giraud, G., 2017. Global Trends in Metal Consumption and Supply: The Raw Material-Energy Nexus. *Elements* 13, 319–324. <https://doi.org/10.2138/gselements.13.5.319>.
- Wanvik, J., 2000. Norwegian anorthosites and their industrial uses, with emphasis on the massifs of the Inner Sogn-Voss area in western Norway.
- Wanvik, J.E., 2010. Summary of knowledge about Norwegian anorthosite prospecting - in relation to Greenland anorthosites | Norges Geologiske Undersøkelse (No. 2010.020). Geological Survey of Norway (NGU).
- World Bank, 2020. Commodity Markets [WWW Document]. World Bank. URL <https://www.worldbank.org/en/research/commodity-markets> (accessed 6.9.21).
- Xiong, Y., 2006. Estimation of medium effects on equilibrium constants in moderate and high ionic strength solutions at elevated temperatures by using specific interaction theory (SIT): Interaction coefficients involving Cl, OH- and Ac-up to 200°C and 400 bars. *Geochem. Trans.* 7, 4. <https://doi.org/10.1186/1467-4866-7-4>.
- Zemaitis, J.F., 1980. Predicting Vapor-Liquid-Solid Equilibria in Multicomponent Aqueous Solutions of Electrolytes, in: *Thermodynamics of Aqueous Systems with Industrial Applications*, ACS Symposium Series. AMERICAN CHEMICAL SOCIETY, pp. 227–246. <https://doi.org/10.1021/bk-1980-0133.ch010>.